A search for thermal X-ray signatures in gamma-ray bursts – II. The *Swift* sample

Martin Sparre[1,2]* and Rhaana L. C. Starling[2]

[1]*Dark Cosmology Centre, Niels Bohr Institute, University of Copenhagen, Juliane Maries Vej 30, 2100 Copenhagen, Denmark*
[2]*Department of Physics and Astronomy, University of Leicester, University Road, Leicester LE1 7RH*

ABSTRACT

In several gamma-ray bursts (GRBs) excess emission, in addition to the standard synchrotron afterglow spectrum, has been discovered in the early-time X-ray observations. It has been proposed that this excess comes from blackbody emission, which may be related to the shock breakout of a supernova in the GRBs progenitor star. This hypothesis is supported by the discovery of excess emission in several GRBs with an associated supernova. Using mock spectra we show that it is only likely to detect such a component, similar to the one proposed in GRB 101219B, at low redshift and in low absorption environments. We also perform a systematic search for blackbody components in all the GRBs observed with the *Swift* satellite and find six bursts (GRBs 061021, 061110A, 081109, 090814A, 100621A and 110715A) with possible blackbody components. Under the assumption that their excess emission is due to a blackbody component we present radii, temperatures and luminosities of the emitting components. We also show that detection of blackbody components only is possible in a fraction of the *Swift* bursts.

Key words: gamma-ray burst: general – supernovae: general.

1 INTRODUCTION

Gamma-ray bursts (GRBs) emit extreme amounts of γ-rays on a short time-scale; typically 10^{50}–10^{54} erg are released in 0.1–100 s. Only violent processes, such as a compact object merger or the collapse of a massive star, can explain these large energy releases, which have made GRBs observable out to high redshifts of $z \approx 8$–9 (Salvaterra et al. 2009; Tanvir et al. 2009; Cucchiara et al. 2011).

There exists strong evidence that the collapse of massive stars can produce long GRBs ($T_{90} > 2$ s; Kouveliotou et al. 1993), since spectroscopic features from supernovae (SNe) have been detected in optical follow-up observations of GRBs (e.g. Galama et al. 1998; Hjorth et al. 2003; Starling et al. 2011; also see review by Hjorth & Bloom 2011). All these SNe are of type Ic with broad lines and no signs of hydrogen or helium. Besides these spectroscopic detections, evidence for SN Ic features is also found in light curves of some GRBs (Patat et al. 2001; Lipkin et al. 2004; Cobb et al. 2010; Cano et al. 2011).

One burst of particular interest was GRB 060218 (Mazzali et al. 2006; Soderberg et al. 2006). It had an associated SN (Pian et al. 2006), and its X-ray afterglow could best be described by a combination of synchrotron emission, which is usual for afterglows, and blackbody emission (Campana et al. 2006). Waxman, Mészáros &

Campana (2007) showed that this blackbody emission could origin in a shock generated by the breakout of an SN through the surface of the GRBs progenitor star. Subsequently, thermal X-ray emission which may be described by a blackbody has been suggested in GRBs 090618, 100316D and 101219B, which all have associated SNe (Page et al. 2011; Starling et al. 2011; Starling et al. 2012, respectively; see also Starling, Page & Sparre 2012). This supports the connection of the blackbody component with emission from an SN. Deviations from a single power law in the early X-ray spectra in GRBs were also found by Butler (2007), who identified a soft emission component in 5–10 per cent of the bursts in the studied sample.

In this series of papers, we search for more bursts with X-ray blackbody components, and derive the conditions under which such components may be reliably recovered. In Paper I (Starling et al. 2012) blackbody components were identified in bursts with spectroscopic or photometric signatures in the optical. The aim of this paper is to perform a systematic search for more bursts with X-ray blackbody components in the *Swift* sample, and to derive the conditions under which such components may be reliably recovered. In Section 2 the sample and model fitting are described, and in Section 3 we create simulated spectra to set constraints on the detectability of blackbody components. In Section 4 bursts are selected as candidates for having blackbody emission, and Section 5 presents and discusses the final list of candidates. Section 6 extracts physical parameters, assuming that the excess emission is blackbody

*E-mail: sparre@dark-cosmology.dk

Table 1. The parameters in the four fitting models (M1–M4). It is shown whether a parameter is free (if marked as *free*), fixed (*fixed*), not included (–) or fitted to the late-time spectrum (*late fit*).

	Description	M1	M2	M3	M4
z	Redshift of the GRB	Fixed	Fixed	Fixed	Fixed
$n_{H,gal}$	Galactic column density	Fixed	Fixed	Fixed	Fixed
$n_{H,int}$ or n_H	Intrinsic column density in the GRB host galaxy	Free	Free	Late fit	Late fit
Γ	Photon index, defined as $F_E \propto E^{-\Gamma}$ (F_E is flux)	Free	Free	Free	Free
F_{PL}	Flux of the power-law component of the afterglow in a 0.3–10 keV band	Free	Free	Free	Free
kT	Blackbody temperature (in the rest frame of the burst)	–	Free	–	Free
F_{BB}	Flux of the blackbody emission in a 0.3–10 keV band	–	Free	–	Free

emission, and the fraction of GRBs with probable excess emission is examined.

For the cosmological calculations we assume a Λ cold dark matter universe with $h_0 = 0.71$, $\Omega_m = 0.27$ and $\Omega_\Lambda = 0.73$. All stated errors and error bars are 90 per cent confident. In the plots n_H is in units of $10^{22}\,\mathrm{cm}^{-2}$ unless stated otherwise. We will use the words *thermal components* and *blackbody components* interchangeably.

2 FITTING MODELS WITH BLACKBODY COMPONENTS TO A SAMPLE OF GRBS

2.1 A sample of *Swift* bursts

The sample, in which we will search for X-ray blackbody components, consists of the GRBs observed with the *Swift* XRT (Burrows et al. 2005), where redshifts are determined with optical spectroscopy, or simultaneous multiband photometry, as obtained from the Gamma-Ray Burst Optical/Near-Infrared Detector (GROND, Krühler et al. 2011a). Furthermore we only select bursts, where windowed timing (WT) mode observations exist, since this assures that data were taken shortly after the trigger. The sample consists of 190 bursts with the most recent burst from 2011 August 8.

We used the publicly available[1] WT mode data, see Evans et al. (2009). Note that the sample also includes bursts not triggered by *Swift*. We make use of the time-averaged WT mode spectra, which have all been created in the same manner according to Evans et al. (2009) and using the *Swift* software version 3.8 and the latest calibration data.

2.2 Spectral modelling

In order to identify blackbody emission for a burst, it is necessary to understand the interplay between all contributing components in the observed spectrum: the afterglow continuum, the blackbody emission and the absorption of the source emission by gas in the line of sight within the host galaxy and the Galaxy. These properties can be parametrized by the seven parameters in Table 1. Note that not all parameters are free: in our sample the redshift of each burst is known, and the Galactic column density can, in most cases, be determined to within ± 5 per cent (Kalberla et al. 2005).

For each burst we fitted four different models to the WT spectrum. These models are also shown in Table 1. Model 1 (M1) is an absorbed power law, whereas Model 2 (M2) also includes blackbody emission at the redshift of the bursts. Models 3 and 4 (M3 and M4) are similar to Models 1 and 2, with the only difference that $n_{H,int}$ is fitted to the late-time photon-counting mode spectrum,

[1] Website for XRT data: http://www.swift.ac.uk/.

which we expect to be free from additional components and therefore a reliable measure of any absorbing column, instead of from the early-time (WT) spectrum itself. The atomic data used are solar abundances from Wilms, Allen & McCray (2000) and cross-sections from Verner et al. (1996).

For all the WT spectra we group the spectra in 20 counts per bin and perform a χ^2 fit. For the late-time observations, used to determine $n_{H,int}$ in Models 3 and 4, ungrouped spectra are fitted with Cash statistics Cash (1979).

2.3 Selecting candidates with the *F*-test

The *F*-test (e.g. Lampton, Margon & Bowyer 1976) is a statistical test, which gives the probability that an improvement in the reduced χ^2, with the inclusion of extra parameters, is due to an improvement in the fitting model. To test whether a blackbody component is present in a spectrum, we therefore use the *F*-test to compare Models 1 and 2 and Models 3 and 4. Protassov et al. (2002) showed that the *F*-test is not a stringent test, but in the following section we will explicitly show that the *F*-test in many cases is sufficient to recover blackbody components, when they are present. In Section 4 we will select the candidates.

3 RECOVERING A BLACKBODY COMPONENT IN MOCK SPECTRA OF GRB 101219B

In Section 4 it will be found that one of the candidates for having a blackbody component is GRB 101219B with a temperature of 0.22 keV in the Model 2 fit (see Section 4 and Table 2). This value is consistent with the value found in Paper I. With a redshift of $z = 0.55$ (de Ugarte Postigo et al. 2011) GRB 101219B is one of the most distant GRBs with a spectroscopically detected SN (Sparre et al. 2011). Now mock spectra will be used to derive the range of column densities, redshifts and afterglow parameters for which a detection of the blackbody component is possible, and we will use this information to refine our candidate list.

3.1 The role of column densities

To reveal the role of the column densities, the *F*-test significances of the blackbody detections are calculated for several 101219B-like mock spectra with n_H values varying from 0.0 to $0.8 \times 10^{22}\,\mathrm{cm}^{-2}$. The other parameters used to create the mock spectra are identical to the recovered value in the fit of Model 2 from the real data.

The left-hand panel in Fig. 1 shows how the *F*-test significance (calculated from Models 1 and 2) depends on the n_H value used to generate the mock spectra. If the *F*-test significance is lower than 10^{-4} we will say that Model 2 is favoured over Model 1 (i.e. the presence of a blackbody component is favoured). The central and

Table 2. The initial candidates for having a blackbody component. Candidates with $z > 3$ are omitted. The *F*-test significances are marked as **bold** if the burst is a candidate in the given model. If the recovered n_H is too uncertain the burst is marked with 'unc. n_H' (see Section 4.1 for details).

GRB	z	F-stat. (M1-2)	F-stat. (M3-4)	kT (M2)	kT (M4)	n_H (M2)	n_H (M4,fixed)	Note
050724	0.257	**2.1×10^{-7}**	Overflow	0.9 ± 0.1	Underflow	0.33 ± 0.06	0.2 ± 0.1	
050820A	2.6147	1.0×10^{-7}	Overflow	$0.4^{+3.6}_{-0.4}$	Underflow	0^{+20}_{-0}	$0.00^{+0.09}_{-0.00}$	Unc. n_H High z
060124	2.3	0.041	3.4×10^{-8}	0.6 ± 0.1	0.46 ± 0.07	0.6 ± 0.1	0.8 ± 0.2	High z
060202	0.783	**4.2×10^{-6}**	**4.3×10^{-14}**	$0.38^{+0.06}_{-0.05}$	0.34 ± 0.03	1.6 ± 0.1	1.7 ± 0.2	
060218	0.0331	**1.0×10^{-174}**	**9.6×10^{-110}**	0.123 ± 0.002	0.186 ± 0.002	0.76 ± 0.02	0.40 ± 0.04	
060418	1.49	**3.0×10^{-6}**	Overflow	0.61 ± 0.05	$0.00^{+0.03}_{-0.00}$	0.5 ± 0.1	$0.2^{+0.3}_{-0.2}$	
060502A	1.5026	5.6×10^{-5}	**4.7×10^{-5}**	0.35 ± 0.04	0.31 ± 0.02	0.4 ± 0.2	0.5 ± 0.2	Unc. n_H (M2 only)
060604	2.68	0.16	2.1×10^{-9}	$0.15^{+0.09}_{-0.02}$	$1.6^{+0.3}_{-0.2}$	$2.2^{+0.7}_{-0.4}$	1.1 ± 0.3	High z
060714	2.7108	0.27	2.0×10^{-9}	$0.24^{+0.06}_{-0.11}$	1.9 ± 0.3	3.0 ± 1.1	$1.1^{+0.6}_{-0.5}$	Unc. n_H High z
060904B	0.7029	**0.0014**	1.0	$0.29^{+0.06}_{-0.05}$	$0.00^{+0.05}_{-0.00}$	$0.53^{+0.07}_{-0.06}$	0.4 ± 0.1	
061021	0.3463	**2.9×10^{-7}**	**3.2×10^{-15}**	$0.12^{+0.03}_{-0.02}$	0.12 ± 0.01	$0.08^{+0.13}_{-0.08}$	0.08 ± 0.02	
061110A	0.7578	**6.5×10^{-11}**	**0.00019**	0.32 ± 0.02	Overflow	0.14 ± 0.04	$0.3^{+0.4}_{-0.3}$	
061121	1.3145	**1.5×10^{-8}**	**1.1×10^{-9}**	0.50 ± 0.06	0.45 ± 0.03	0.5 ± 0.1	0.61 ± 0.08	
070318	0.8397	0.0075	**9.9×10^{-11}**	0.3 ± 0.1	0.24 ± 0.04	$0.6^{+0.2}_{-0.1}$	0.8 ± 0.1	
070419A	0.9705	0.17	1.2×10^{-7}	0.4 ± 0.1	0.18 ± 0.04	0.5 ± 0.1	$0.8^{+1.7}_{-0.8}$	Unc. n_H
070508	0.82	**1.0×10^{-5}**	0.074	$0.066^{+0.002}_{-0.004}$	$0.030^{+0.002}_{-0.001}$	$1.12^{+0.09}_{-0.07}$	0.6 ± 0.2	
070724A	0.457	0.15	**0.0014**	$0.15^{+0.10}_{-0.04}$	$0.8^{+0.2}_{-0.1}$	1.0 ± 0.5	$0.1^{+0.3}_{-0.1}$	
071031	2.6918	6.1×10^{-9}	8.4×10^{-67}	$2.1^{+0.4}_{-0.3}$	1.44 ± 0.06	0.9 ± 0.1	$0.0^{+0.7}_{-0.0}$	High z
071112C	0.8227	**0.00011**	**0.00013**	$0.40^{+0.06}_{-0.07}$	$0.37^{+0.03}_{-0.04}$	$0.08^{+0.08}_{-0.07}$	$0.1^{+0.2}_{-0.1}$	
080210	2.6419	0.10	0.0020	$1.0^{+0.3}_{-0.2}$	$1.0^{+0.3}_{-0.2}$	$1.0^{+1.2}_{-1.0}$	$1.5^{+0.8}_{-0.7}$	Unc. n_H High z
080310	2.4274	0.052	1.7×10^{-22}	$2.0^{+1.1}_{-0.7}$	1.3 ± 0.1	$0.63^{+0.07}_{-0.09}$	$0.4^{+0.3}_{-0.2}$	High z
080319B	0.9382	**1.4×10^{-25}**	1.0	$1.02^{+0.08}_{-0.07}$	Underflow	0.12 ± 0.01	$0.08^{+0.04}_{-0.03}$	
080413A	2.433	0.27	2.0×10^{-7}	$0.14^{+0.04}_{-0.03}$	1.0 ± 0.1	$2.8^{+0.9}_{-0.6}$	$0.5^{+1.0}_{-0.5}$	Unc. n_H High z
080430	0.767	**0.00020**	**3.3×10^{-5}**	0.24 ± 0.06	0.21 ± 0.03	$0.3^{+0.3}_{-0.1}$	0.36 ± 0.06	
080603B	2.6892	0.042	2.8×10^{-13}	$1.7^{+0.6}_{-0.3}$	$1.6^{+0.2}_{-0.1}$	0.8 ± 0.3	$0.2^{+0.6}_{-0.2}$	Unc. n_H High z
080604	1.4171	**0.0010**	**3.0×10^{-6}**	$0.34^{+0.06}_{-0.10}$	0.28 ± 0.04	$0.04^{+0.21}_{-0.04}$	$0.2^{+0.5}_{-0.2}$	
080605	1.6403	**0.00011**	0.84	$0.087^{+0.020}_{-0.006}$	$0.04^{+0.09}_{-0.04}$	$1.2^{+0.2}_{-0.1}$	0.6 ± 0.3	
080721	2.5914	2.6×10^{-10}	5.3×10^{-51}	$0.21^{+0.01}_{-0.02}$	2.0 ± 0.1	2.2 ± 0.3	0.5 ± 0.2	Unc. n_H High z
080805	1.5042	0.38	1.1×10^{-7}	$0.06^{+0.05}_{-0.02}$	0.27 ± 0.05	$0.65^{+0.16}_{-0.07}$	1.2 ± 0.5	Unc. n_H
080928	1.6919	**2.9×10^{-5}**	overflow	$1.7^{+0.4}_{-0.3}$	Underflow	0.5 ± 0.1	0.3 ± 0.1	
081007	0.5295	0.0016	**0.00032**	$0.20^{+0.07}_{-0.05}$	0.30 ± 0.03	$0.8^{+0.3}_{-0.2}$	0.5 ± 0.1	Unc. n_H (M2 only)
081008	1.967	0.057	**6.7×10^{-33}**	2.1 ± 0.8	$1.19^{+0.08}_{-0.07}$	0.9 ± 0.1	0.3 ± 0.3	
081109	0.9787	0.047	**1.0×10^{-5}**	$1.0^{+0.3}_{-0.2}$	0.13 ± 0.04	0.5 ± 0.1	1.0 ± 0.2	
081203A	2.05	0.00073	0.053	0.5 ± 0.08	Overflow	1.4 ± 0.5	2^{+2}_{-1}	Unc. n_H High z
081222	2.77	0.086	2.9×10^{-5}	$0.16^{+0.05}_{-0.07}$	$1.3^{+0.3}_{-0.2}$	$1.0^{+0.4}_{-0.3}$	0.4 ± 0.2	High z
081230	2.03	0.12	0.00023	$2.8^{+0.7}_{-1.0}$	1.5 ± 0.4	$0.8^{+0.4}_{-0.3}$	0.2 ± 0.2	High z
090418A	1.608	0.062	**8.3×10^{-5}**	0.5 ± 0.2	0.27 ± 0.09	$0.5^{+0.6}_{-0.3}$	1.1 ± 0.2	
090424	0.544	**0.0041**	**0.0042**	$1.5^{+0.2}_{-0.3}$	1.3 ± 0.2	$0.44^{+0.03}_{-0.02}$	0.42 ± 0.06	
090618	0.54	**0.00026**	**4.1×10^{-6}**	1.9 ± 0.2	$0.38^{+0.04}_{-0.03}$	0.26 ± 0.02	0.19 ± 0.02	
090809	2.737	0.020	4.3×10^{-7}	0.21 ± 0.03	2.1 ± 0.3	6 ± 1	0.6 ± 0.3	High z
090812	2.452	1.5×10^{-5}	1.9×10^{-8}	$1.5^{+0.5}_{-0.2}$	0.10 ± 0.02	$0.8^{+0.2}_{-0.1}$	$1.2^{+0.7}_{-0.6}$	High z
090814A	0.696	**1.6×10^{-10}**	**1.3×10^{-10}**	0.28 ± 0.03	0.26 ± 0.01	0.14 ± 0.06	$0.2^{+0.3}_{-0.2}$	
090926B	1.24	2.9×10^{-9}	1.8×10^{-9}	0.53 ± 0.07	0.52 ± 0.04	$1.5^{+0.3}_{-0.2}$	$1.5^{+1.2}_{-0.8}$	Unc. n_H
091029	2.752	2.0×10^{-5}	0.0054	$0.38^{+0.08}_{-0.07}$	overflow	$1.0^{+0.7}_{-0.5}$	0.5 ± 0.2	Unc. n_H High z
100117A	0.92	0.0055	1.7×10^{-10}	$1.2^{+0.4}_{-0.2}$	0.09 ± 0.2	0.2 ± 0.2	$2.2^{+1.6}_{-1.2}$	Unc. n_H
100418A	0.6235	**0.00074**	**2.3×10^{-11}**	$0.21^{+0.03}_{-0.04}$	0.24 ± 0.01	0.2 ± 0.1	$0.1^{+0.4}_{-0.1}$	
100621A	0.542	**0.00011**	**2.7×10^{-5}**	$0.48^{+0.05}_{-0.06}$	$0.29^{+0.03}_{-0.04}$	1.4 ± 0.2	2.0 ± 0.2	
101219B	0.55	**2.2×10^{-13}**	**3.9×10^{-27}**	0.22 ± 0.03	0.20 ± 0.1	$0.06^{+0.06}_{-0.05}$	0.1 ± 0.1	
110205A	2.22	0.021	4.7×10^{-10}	3 ± 1	$1.6^{+0.3}_{-0.2}$	$0.54^{+0.08}_{-0.10}$	0.4 ± 0.1	High z
110715A	0.82	0.40	**6.6×10^{-6}**	$0.15^{+0.06}_{-0.08}$	$0.15^{+0.04}_{-0.03}$	1.0 ± 0.4	1.3 ± 0.3	
110731A	2.83	0.22	0.0049	$0.12^{+0.07}_{-0.04}$	$1.7^{+0.6}_{-0.5}$	1.8 ± 0.3	$1.1^{+0.7}_{-0.6}$	Unc. n_H High z
110808A	1.348	0.0017	0.00068	0.29 ± 0.07	$0.22^{+0.02}_{-0.03}$	$0.2^{+0.3}_{-0.2}$	$0.6^{+0.4}_{-0.3}$	Unc. n_H

[a] Only for Model 2.

the right-hand panels show the n_H and kT recovered by the fits of the same mock spectra. When the n_H used to generate the mock data is larger than 0.4×10^{22} cm^{-2}, the n_H recovered by the fit is often too small, and in most cases a temperature with a large error is recovered. For $n_H < 0.4 \times 10^{22}$ cm^{-2} the F-test favours the existence of a blackbody component, and correct kT and n_H values are recovered within their errors.

Similar mock spectra without blackbody components were also made, and no significant detections of blackbody components were favoured by the F-test.
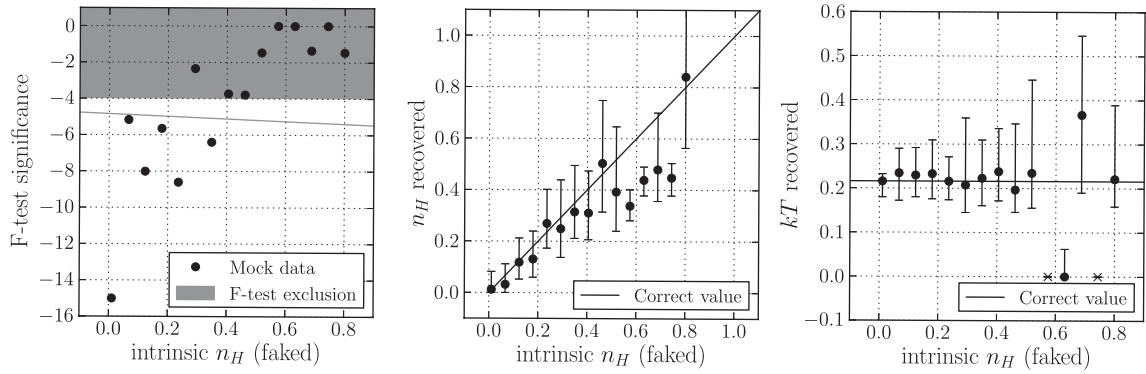
Figure 1. Left: the *F*-test significance of the recovery of a 101219B-like blackbody component as a function of n_H (in units of 10^{22} cm^{-2}). Central: the n_H value recovered (in the Model 2 fit) as a function of the correct n_H. Right: the recovered temperature (in keV).

3.1.1 Fixing n_H to the late-time spectrum

For the fits of the real data the n_H values in Models 3 and 4 are fixed to the fitted value from the late-time spectrum. Now it will explicitly be shown that this method might lead to significant blackbody detections for spectra with no real blackbody components, when n_H is fixed to a too large value.

First spectra with photon indices and power-law normalizations identical to GRB 101219B are generated, but with n_H varying from 0 to 0.8×10^{22} cm^{-2}. All the spectra are generated without blackbody components. In the fitting function n_H is fixed to 0.5×10^{22} cm^{-2} for all the spectra, just like if this value had come from the fit of a late-time spectrum. In Fig. 2 (left-hand panel) it is shown that the *F*-test favours a blackbody component when $n_H \lesssim 0.35 \times 10^{22}$ cm^{-2}. All the recovered blackbody components had temperatures between 0.08 and 0.2 keV. We conclude that if n_H is fixed to a value of $\sim 0.15 \times 10^{22}$ cm^{-2} larger than the real value, a spurious blackbody component will compensate for the flux lost due to the high column density absorption parameter.

A side result of this analysis is that typical Galactic column densities cannot lead to spurious detections of blackbody components. $n_{H,gal}$ is typically of the order of $\sim 0.05 \times 10^{22}$ cm^{-2} with a 10 per

cent error (Kalberla et al. 2005), which is well below the critical value of 0.15×10^{22} cm^{-2} found above.

3.2 Redshift and afterglow parameters

To find the redshifts for which it is possible to observe a GRB 101219B-like blackbody component, simulations like those in Section 3.1 are performed, with the only difference that z is varied instead of n_H. Fig. 2 (central panel) shows that blackbody components are recovered with *F*-test significances $\lesssim 10^{-8}$ when $z < 1$. For $1 < z < 2$ the significances of the detections are lowered by several orders of magnitudes.

The role of the parameters describing the synchrotron emission from the afterglow will now be quantified. First we fix the photon index to the GRB 101219B value and simulate spectra with power-law normalizations covering the values observed in our sample. The resulting *F*-test significances of our fits are shown in Fig. 2 (right-hand panel). A low normalization constant is essential in order not to dilute the signal from the blackbody component with noise from the afterglow emission. We also fitted simulated spectra with a fixed normalization and a varying photon index, see Fig. 3. A trend in
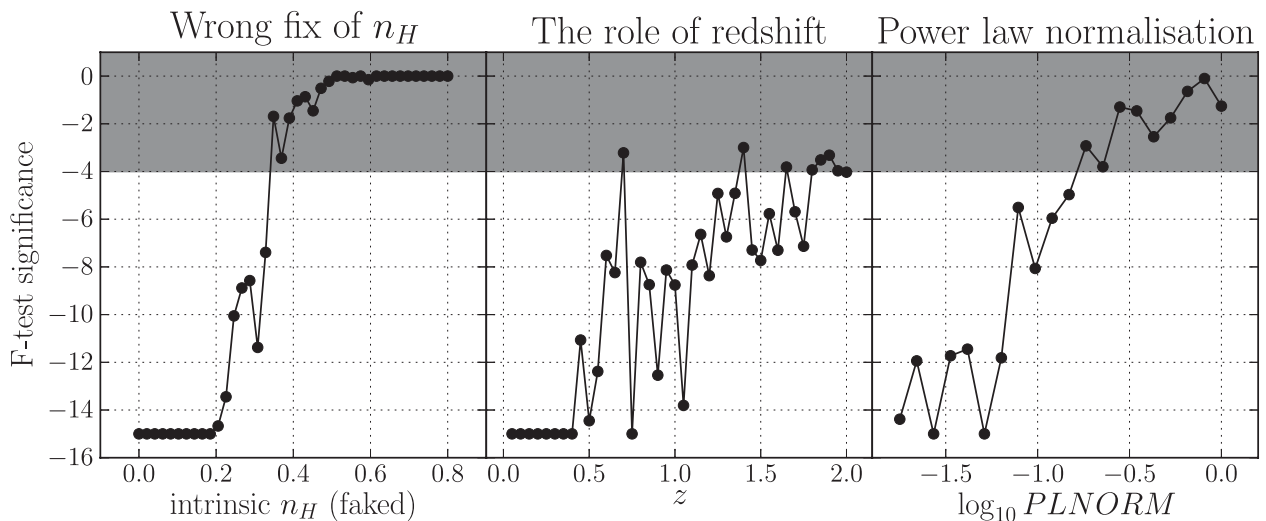

Figure 2. Left: in the fits the n_H value is fixed to 0.5×10^{22} cm^{-2}, which is different from the n_H used the generate the spectra, shown as abscissa. Spurious detections appear, when n_H is fixed to a large value. Central: the *F*-test significance as a function of z for a GRB 101219B-like burst. Right: the role of the power-law normalization (in arbitrary units).
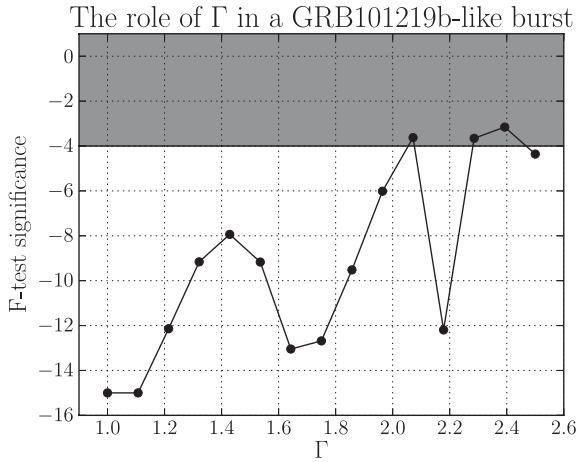
Figure 3. The *F*-test significance as a function of the photon index.

the complicated pattern is that GRB 101219B-like black bodies are most likely to be detected with low photon indices.

4 SELECTING CANDIDATES

Now we will start searching for candidates with blackbody components in our sample. The bursts with *F*-test probabilities lower than 0.005 in the Models 1 and 2 comparison or the Models 3 and 4 comparison were selected. For now, we are only interested in making an initial list of candidates, which will be refined later. We are therefore using a looser *F*-test significance threshold here than in Section 3 (a limit of 0.005 is now used instead of 10^{-4}). The selected candidates are listed in Table 2.

4.1 Ruling out candidates with uncertain n_H

It is important to understand the contribution of n_H in order to make a reliable detection of a blackbody component. We therefore removed all bursts with a 90 per cent error on n_H larger than 0.4×10^{22} cm^{-2} for Model 2 or larger than 0.8×10^{22} cm^{-2} for Model 4. A lower threshold was chosen for Model 2, so candidates with a degenerate n_H value were excluded. In Table 2 a burst is marked with *uncertain n_H*, if it is excluded due to this criterion. The analysis was done for larger values of the thresholds, but it did not lead to the detection of more candidates in the refined analysis, which will be presented in Sections 4.3 and 4.4.

4.2 Candidates at high and low redshift

4.2.1 The high-redshift candidates (z > 2)

For $z > 2$ GRB 101219B-like blackbody components are difficult to detect (see Section 3.2 and Fig. 2). A number of candidates with $z > 2$ have, however, emerged in our analysis. They typically exhibit high temperatures ($kT \gtrsim 1$ keV), which is much higher than most previously claimed examples (e.g. Campana et al. 2006; Starling et al. 2011). They also have an uncertain n_H, which increases the risk of a spurious detection.

At low redshift (e.g. $z < 1$), only a few candidates have temperatures larger than 1 keV, even though a detection of such a blackbody component is expected to be easier at lower redshift. The high-redshift candidates are therefore unlikely to represent real black bodies, and they will not be examined further in this work.
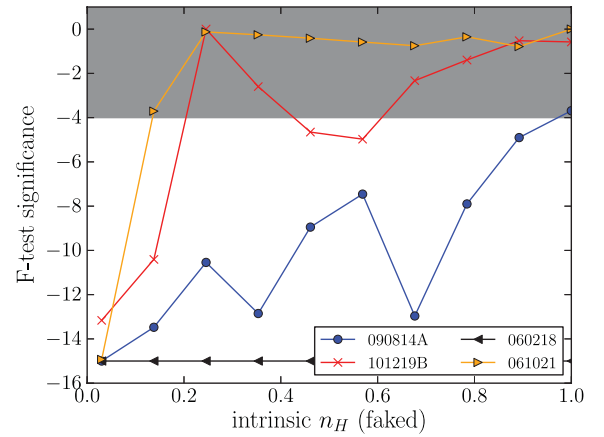
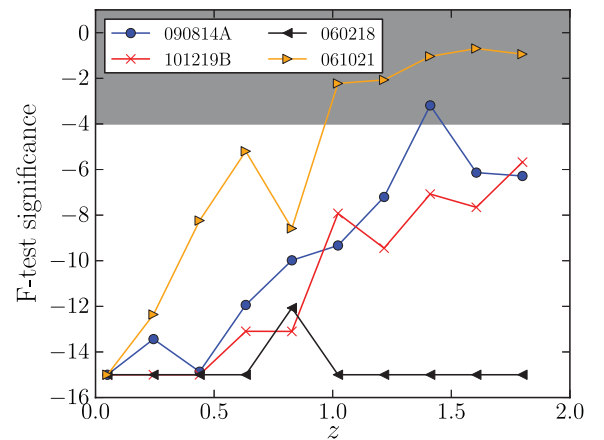**Figure 4.** Same as Fig. 1 (left), but with three additional bursts.

Figure 5. Same as Fig. 2 (central), but with three additional bursts.

4.2.2 The low-redshift candidates (z < 2)

Three of the candidates, GRBs 060218, 090618 and 101219B, already have identified blackbody components in other studies, and they also have a spectroscopically confirmed SN in the optical. Among our candidates is also GRB 100418A, which also has an SN in the optical (de Ugarte Postigo et al. in preparation). Paper I studied the early X-ray spectrum of GRB 100418, and also find that a model with a power law and a blackbody model can give a good fit. However, they cannot rule out an absorbed power-law model given the large uncertainty on the intrinsic absorbing column of this GRB host, which may be higher than the limit for detectability we find in Section 3.1 of 0.4×10^{22} cm^{-2}. Paper I also studied GRB 081007, and found an indication of a blackbody component, but no conclusive evidence.

At first sight it is worrying that GRB 100316D, which Starling et al. (2011) showed had an excess blackbody emission, is not among our candidates. An examination of this burst shows that it is not selected due to a *F*-test value of 0.007 (for the Models 1 and 2 comparison), which is slightly above our threshold of 0.005 defined in Section 2.3. It is therefore clear that our candidate selection algorithm will not find all bursts with blackbody components (discussed further in Section 6.1).

Figs 4 and 5 show how the *F*-test significances of the blackbody component detections in a selection of our low-redshift candidates depend on column density and redshift. In general the same trends found for GRB 101219B above apply for both GRBs 090814A and

061021. A blackbody component, similar to the one present in GRB 060218, is expected to be detectable at high redshifts (e.g. $z \gtrsim 2$).

4.3 Approach I: fitting with five free parameters

The final step in our selection procedure is to do a time-sliced analysis of the remaining candidates, i.e. those without remarks in Table 2. In this section we will focus on the candidates selected in the comparison between Models 1 and 2. In Section 4.4 we will fit and analyse the candidates selected with Models 3 and 4.

For each of the candidates, where Model 2 is favoured by the i-test, we manually inspected the light curves, and selected time intervals, where the light curves exhibit a single power-law decay. We especially tried to avoid time intervals with flares and plateaus.

To each time-sliced spectrum all the models were fitted, see a summary of the fits in Table 3. Several candidates with no flare–free epochs are excluded from the table. The candidates with excess emission are GRBs 061021, 061110A and 090814A. They have low column densities ($n_H < 0.3 \times 10^{22}$ cm^{-2}) for both Model 2, where the n_H is a free parameter, and Model 4, where n_H is fitted with the late-time spectrum. In all the fits the presence of a blackbody component is favoured by the F-test with significances from 0.0005 to 2.4×10^{-13}. The temperatures are between 0.1 and 0.3 keV, which is consistent with claimed blackbody components in other studies.

In Table 3, some bursts are also listed as candidates with some caveats. These are GRB 100621A (because it has an F-test significance of 0.00144, and a large n_H), GRB 061121 (it has large kT and z, and the i-test does not favour a blackbody component in Models 3

and 4) and GRB 050724 (it has an unexpectedly high kT). We note that GRB 050724 has been classified as a short burst with extended emission (Barthelmy et al. 2005), so its origins may not lie in the collapse of a massive star as is the case for the rest of our sample which are all long GRBs.

4.4 Approach II: breaking N_H degeneracies with the late-time spectrum

The three bursts, which were candidates for having blackbody components in the previous subsection, all have low column densities $n_H < 0.3 \times 10^{22}$ cm^{-2}. This is expected from Fig. 4 which shows that it is hard to recover a blackbody component at large n_H, when it is fitted as a free parameter (as in Models 1 and 2).

We will now do a new search for blackbody components, where we use the late-time spectrum to fit n_H, i.e. use Models 3 and 4. This method can break the degeneracies between n_H and the other parameters, but it also has the disadvantage that a spurious blackbody component can be found if a too high value of n_H is recovered in the late-time spectrum (see Section 3.1.1).

We fitted Models 3 and 4 to the candidates. Table 4 summarizes the fits. Several of the candidates are not shown in the table, since they have complex and bumpy light curves, or too little data to extract a good spectrum.

Several bursts have favourable F-test significances. To explicitly check whether the fixing of n_H might have caused spurious blackbody detections, we made additional fits, where n_H was fixed to a range of different values within the 90 per cent confidence intervals recovered in the late-time fits. Fig. 6 shows how the

Table 3. The time-sliced fits from Section 4.3, where bursts are selected with Models 1 and 2. Three reliably detected blackbody components are found.

GRB	z	Time	F-test M1−2	F-test M3−4	kT (M2)	kT (M4)	n_H (M2)	n_H (M4,fixed)
Candidates with probable excess emission								
061021	0.3663	87−170	3.1×10^{-7}	2.4×10^{-13}	$0.13^{+0.03}_{-0.02}$	0.13 ± 0.01	$0.08^{+0.13}_{-0.08}$	0.08 ± 0.02
061110A	0.7578	180−240	2.5×10^{-6}	0.00050	0.25 ± 0.01	0.19 ± 0.01	$0.00^{+0.07}_{-0.00}$	$0.3^{+0.3}_{-0.2}$
090814A	0.696	166−265	4.0×10^{-7}	2.2×10^{-9}	0.32 ± 0.03	0.30 ± 0.01	0.12 ± 0.06	$0.2^{+0.3}_{-0.2}$
090814A	0.696	265−390	1.1×10^{-6}	2.1×10^{-8}	$0.19^{+0.05}_{-0.04}$	0.20 ± 0.02	$0.2^{+0.2}_{-0.1}$	$0.2^{+0.3}_{-0.2}$
Candidates with some caveats								
050724	0.257	100−190	1.3×10^{-6}	−	0.9 ± 0.1	−	0.36 ± 0.09	0.2 ± 0.1
061121	1.3145	125−215	1.1×10^{-5}	1	$0.44^{+0.05}_{-0.06}$	$0.0^{+0.1}_{-0.0}$	0.6 ± 0.1	0.61 ± 0.07
100621A	0.542	80−120	0.022	0.86	$0.69^{+0.06}_{-0.07}$	0.05 ± 0.05	$1.4^{+0.6}_{-0.3}$	2.0 ± 0.2
100621A	0.542	190−230	0.0014	6.0×10^{-7}	0.33 ± 0.06	0.25 ± 0.03	$1.3^{+0.4}_{-0.3}$	2.0 ± 0.2
Candidates where a blackbody component is not favoured								
060202	0.783	148−303	0.0023	0.12	$0.42^{+0.07}_{-0.06}$	$0.045^{+0.003}_{-0.002}$	1.6 ± 0.1	1.7 ± 0.2
060202	0.783	745−1000	0.28	0.0058	overflow	$0.25^{+0.08}_{-0.06}$	1.6 ± 0.2	1.7 ± 0.2
060418	1.49	240−450	0.29	0.20	0.6 ± 0.2	$0.6^{+0.2}_{-0.1}$	0.2 ± 0.2	$0.2^{+0.3}_{-0.2}$
070508	0.82	200−500	0.19	0.17	$0.06^{+0.09}_{-0.02}$	0.031 ± 0.002	$1.0^{+0.3}_{-0.1}$	0.6 ± 0.2
070508	0.82	500−1000	0.055	0.33	$1.0^{+0.8}_{-0.2}$	$0.030^{+0.014}_{-0.004}$	0.8 ± 0.2	0.6 ± 0.2
071112C	0.8227	89−179	0.022	Undef.	$0.40^{+0.08}_{-0.09}$	$0.00^{+0.04}_{-0.00}$	0.2 ± 0.1	$0.1^{+0.2}_{-0.1}$
080319B	0.9382	200−500	0.0077	1.0	$1.0^{+0.4}_{-0.2}$	$0.00^{+0.03}_{-0.00}$	0.13 ± 0.03	0.08 ± 0.03
080430	−							
080604	1.4171	125−200	0.14	0.059	$0.21^{+0.15}_{-0.06}$	$0.27^{+0.06}_{-0.07}$	$0.3^{+0.4}_{-0.3}$	$0.2^{+0.5}_{-0.2}$
080605	1.6403	300−700	0.054	1.0	$0.084^{+0.004}_{-0.008}$	$0.003^{+0.094}_{-0.003}$	$1.3^{+0.2}_{-0.1}$	0.6 ± 0.2
080928	1.6919	280−320	0.0014	Undef.	$2.3^{+0.9}_{-0.6}$	$0.0^{+0.1}_{-0.0}$	0.7 ± 0.3	0.3 ± 0.1
090424	0.544	700−1000	0.62	0.017	$1.1^{+0.8}_{-0.4}$	0.8 ± 0.2	0.52 ± 0.07	0.42 ± 0.05

Table 4. The time-sliced fits from Section 4.4, where bursts are selected with Models 3 and 4. Three reliably detected blackbody components are found.

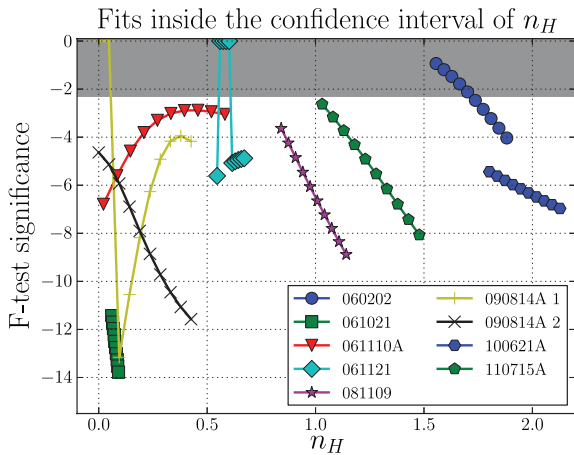| GRB	z	Time	F-test M3$-$4	kT (M4)	n_H (M4,fixed)
Candidates with probable excess emission					
061021	0.3463	87$-$170	2.4×10^{-13}	0.13 ± 0.01	0.08 ± 0.02
061110A	0.7578	180$-$240	0.00050	0.19 ± 0.01	$0.3^{+0.3}_{-0.2}$
081109	0.9787	90$-$200	6.3×10^{-7}	0.16 ± 0.03	$1.0^{+0.2}_{-0.1}$
090814A	0.696	166$-$265	2.2×10^{-9}	0.30 ± 0.01	0.3 ± 0.2
090814A	0.696	265$-$390	2.1×10^{-8}	0.20 ± 0.02	0.2 ± 0.2
100621A	0.542	80$-$120	0.86	0.05 ± 0.05	2.0 ± 0.2
100621A	0.542	190$-$230	6.0×10^{-7}	0.25 ± 0.03	2.0 ± 0.2
110715A	0.82	97$-$501	6.6×10^{-6}	0.15 ± 0.03	1.3 ± 0.2
Candidates with some caveats					
060202	0.783	148$-$303	0.12	$0.045^{+0.004}_{-0.002}$	1.7 ± 0.2
060202	0.783	745$-$1000	0.0058	$0.25^{+0.07}_{-0.06}$	1.7 ± 0.2
061121	1.3145	125$-$215	7.5×10^{-6}	0.43 ± 0.03	$0.61^{+0.07}_{-0.06}$
Candidates where a blackbody component is not favoured					
071112C	0.8227	89$-$179	Undef.	$0.00^{+0.04}_{-0.00}$	$0.1^{+0.2}_{-0.1}$
080604	1.4171	125$-$200	0.059	0.3 ± 0.1	$0.2^{+0.5}_{-0.2}$
090424	0.544	700$-$1000	0.017	0.8 ± 0.2	0.42 ± 0.05

Figure 6. In Models 3 and 4 n_H is fixed to a value determined from late-time observations. This figure examines how the F-test significances of the candidates from Table 4 depend on n_H values with the 90 per cent confidence intervals found in the fits of the late-time spectra.

significances of the detections depend on the value to which n_H is fixed. The detection is not robust for GRBs 060202 and 061121 because of degeneracies between kT and n_H from the late-time spectrum. The list of candidates from the Models 3 to 4 comparison consists of GRBs 061021, 061110A, 081109, 090814A, 100621A and 110715A.

5 THE FINAL CANDIDATES AND POTENTIAL CAVEATS

We will refer to the bursts in Table 4 as our final list of candidates for having a blackbody component. In this section we will discuss potential caveats for each candidate.

5.1 The redshifts

It is essential that the redshift, which is a fixed parameter in all our models, is reliably determined. Table 5 summarizes how the

redshift has been found for the bursts with excess emission. GRBs 061021, 090814A and 110715 have redshifs found with only two absorption lines. It is however possible that these absorption lines come from other galaxies than the host galaxy of the bursts. The remaining bursts have more reliably determined redshifts with several absorption and/or emission lines.
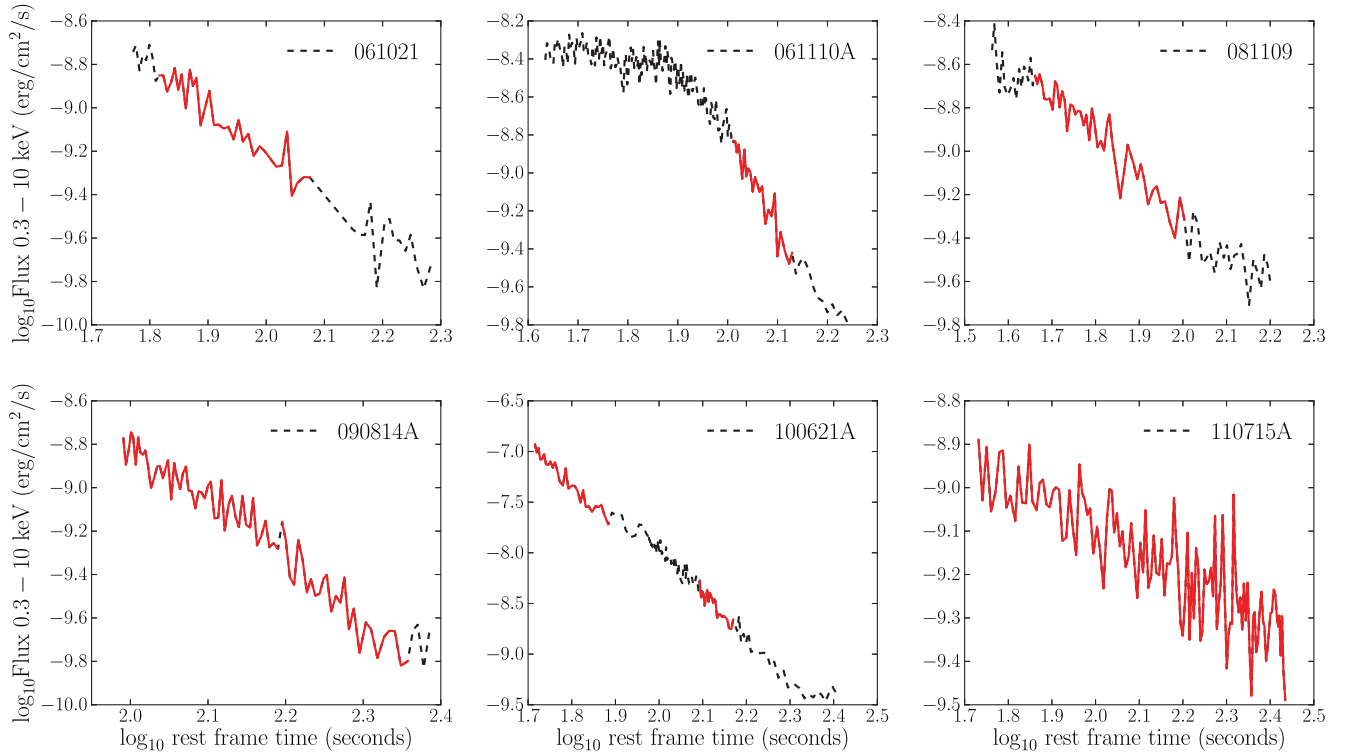
5.2 Light curves and spectral evolution

Fig. 7 shows the parts of the light curves which were used in the time-sliced analysis of the final candidates. We tried to avoid achromatic and X-ray flares and effects from flattening of the light curves, when the time intervals were selected, but we note that evolution of the spectral parameters, the power-law index and/or the blackbody temperature and normalization may be occurring during any of our spectra. When analysing time-sliced spectra this risk is lowered, and we examined the hardness ratios in the XRT repository in order to flag incidences of strong spectral evolution. GRBs 061021, 061110A, 090814A and 110715A have approximately constant hardness ratios in the intervals where time-sliced spectra were analysed. GRB 081109 shows a slowly hardening spectrum, while GRB 100621A becomes significantly softer during the first time slice but shows no spectral evolution during our second time slice. Therefore, the parameters we derive in Table 6 for these latter two GRBs should be considered more uncertain than the error bars allow. Evolution of the blackbody component has been demonstrated for GRBs 060218 (e.g. Campana et al. 2006), 090618 (Page et al. 2011), 100316D (Starling et al. 2011; Olivares et al. 2012) and 101219B (Paper I), where the blackbody cools and expands with time, but typically this evolution is slow compared with the exposure times covered by our X-ray spectra.

5.3 Contribution from the prompt emission

It is important that the prompt emission, which has a spectrum peaking at the energy, E_{peak}, is not entering our X-ray spectrum for the *Swift* XRT (0.3–10 keV), since this potentially could give features resembling blackbody components. Here is a summary of the measurement of E_{peak} for each burst.

Table 5. A schematic summary of how the redshift has been determined for each of the final candidates for having blackbody components.

GRB	Redshift	Absorption lines	Emission lines	References
061021	0.3463	Mg II 2796, Mg II 2803	–	Fynbo et al. (2009)
061110A	0.7578	Mg II 2796, Mg II 2803	Hβ, [O III] doublet	Fynbo et al. (2009)
081109	0.9787	–	GROND photometry	Krühler et al. (2011b)
090814A	0.696	Mg II and Ca II	–	Jakobsson et al. (2009)
100621	0.542	–	[O II] 3727, Hβ, [O III] doublet	Milvang-Jensen et al. (2010); Krühler et al. (2011b)
110715A	0.82	Ca II, Ca I	–	Piranomonte et al. (2011)

Figure 7. The light curves for each of the bursts with probable excess emission. The curve is red (and solid) in the intervals selected for a time-sliced analysis.

Table 6. Radii, temperatures and luminosities of the blackbody components of the final candidates. Candidates from this work and other works are shown. If a value is **bold**, it has been calculated using Stefan–Boltzmann's law (see equation 1), from the two non-bold values for a given candidate. If a E_{iso} value is underlined, it has been calculated from the fluence in the 15–150 keV band and it should only be seen as a lower limit.

GRB	Radius (m)	kT (keV)	L (10^{47} erg s^{-1})	Ref.	z	Time (s)	T_{90} (s)	E_{iso} (erg)
061021	**6.6×10^{10}**	0.13	1.4	This work	0.3663	87−170	46	4.6×10^{51}
061110A	**1.4×10^{11}**	0.19	25.6	This work	0.7578	180−240	41	$\underline{2.9 \times 10^{51}}$
081109	**2.0×10^{11}**	0.16	27.1	This work	0.9787	90−200	190	$\underline{1.8 \times 10^{52}}$
090814A	**3.1×10^{10}**	0.30	8.4	This work	0.696	166−265	80	$\underline{2.8 \times 10^{51}}$
090814A	**4.7×10^{10}**	0.20	3.7	This work	0.696	165−390	80	$\underline{2.8 \times 10^{51}}$
100621A	**8.7×10^{10}**	0.25	32.4	This work	0.542	190−230	64	2.8×10^{52}
110715A	**2.7×10^{11}**	0.15	43.0	This work	0.82	97−501	13	4.1×10^{52}
060218	1.0×10^{10}	0.20	**0.2**	Campana et al. (2006)	0.033	200	2100	6.2×10^{49}
090618	3.0×10^{10}	1.00	1000.0	Page et al. (2011)	0.54	150	113	2.5×10^{53}
090618	1.0×10^{11}	0.20	100.0	Page et al. (2011)	0.54	250	113	2.5×10^{53}
100316D	**3×10^{10}**	0.14	0.3	Starling et al. (2011)	0.0591	250	>1300	3.9×10^{49}
101219B	**2.4×10^{10}**	0.20	1.0	Paper I	0.5519	250	34	4.2×10^{51}

061021. E_{peak} was measured to lie above 540 keV up to 8 s after the trigger (Golenetskii et al. 2006). This is well above XRT energies.

061110A. No spectral break or cut-off was seen with *Swift*/Burst Alert Telescope (BAT), so no E_{peak} information is present. The role of the prompt emission remains unknown for this burst.

090814A. No spectral break or cut-off was seen by *Swift*/BAT. The role of the prompt emission remains unknown for this burst.

081109. *Fermi*/Gamma-ray Burst Monitor (GBM) measured $E_{peak} = 240 \pm 60$ keV (von Kienlin 2008) after 26 s. Our spectrum is well below that energy.

100621A. Konus-Wind fit their spectrum covering 0–74 s with $E_{peak} = 95^{+18}_{-13}$ keV (Golenetskii et al. 2010). Our spectrum starts at 80 s, so probably the peak energy was still well above the XRT band.

110715A. 1 s after trigger Konus–wind measured $E_{peak} = 120^{+12}_{-11}$ keV (Golenetskii et al. 2011), and BAT found 120 ± 21 keV (Ukwatta et al. 2011). It is unlikely that this affects our XRT spectrum, which starts at 98 s.

5.4 Is it a blackbody component?

The six bursts in our final candidate list (GRB 061021, GRB 061110A, GRB 081109, GRB 090814A, GRB 100621A and GRB 110715A) are clearly special, since models with a blackbody component included give better fits than absorbed power laws. We do, however, not have conclusive evidence that the actual emission mechanism is a blackbody component. Other possible explanations could be a model with multiple absorption components at different redshifts, the prompt emission peak could be moving through the band, there could be strong spectral evolution or the determined redshift could be wrong. We have a total of 190 bursts in our sample, so some of them will likely be affected by such features. Due to these caveats we will not report *discovery of blackbody emission*, but instead we will report the finding of bursts with *possible blackbody emission*.

6 PROPERTIES OF THE BLACKBODY COMPONENTS

In this section, we will assume that the actual mechanism behind the excess emission in the spectra of the six bursts is a single-temperature blackbody component. Table 6 shows radius (assuming spherical symmetry) and temperature for these bursts together with values reported in other studies. For our final candidates the radii are calculated from the fitted temperature and luminosity. In the calculation we assume a spherically symmetric blackbody, in thermal equilibrium, which can be described by the Stefan–Boltzmann law:

$$L(\text{erg s}^{-1}) = 1.105 \times 10^{29} \times r^2(\text{m}) \times T^4(\text{keV}). \quad (1)$$

Also note that the luminosities and radii in the table are lower limits, since only the photons in a 0.3–10 keV are included in the luminosity calculation. Due to these caveats, the values in the table should be seen as rough estimates only.

The bursts have temperatures in the range of 0.1–0.3 keV, which is consistent with the previously proposed blackbody components in the time-averaged WT spectra of GRBs 060218, 090618, 100316D and 101219B. They also have luminosities consistent with these
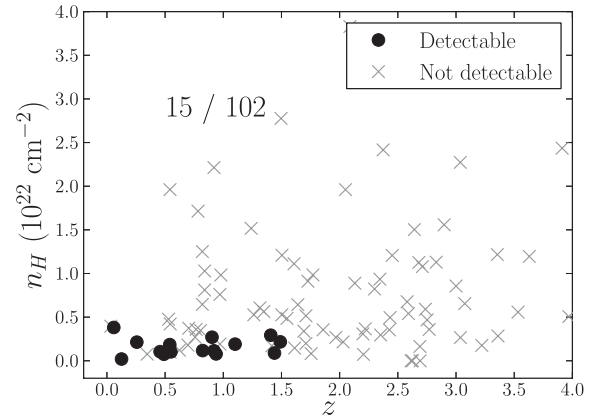

Figure 8. n_H versus z for all the successfully fitted bursts. If a blackbody component, like the one present in GRB 101219B, is detectable in a GRB it is marked with a *black circle*. In 15 out of 102 bursts it is possible to recover such a blackbody component.

previously studied bursts, whereas the radii are slightly larger for GRBs 061110A, 081109 and 110715A than the previously claimed examples.

In the case of GRB 060218 several studies (Ghisellini, Ghirlanda & Tavecchio 2007b,a; Chevalier & Fransson 2008; Li 2007) disfavour the scenario that the excess emission is due to a blackbody component, since they cannot explain the large blackbody luminosities. All our bursts with possible blackbody emission have a luminosity larger than GRB 060218 (Table 6), so they might suffer from a similar problem.

All the bursts have durations (T_{90}) between 13 and 190 s, which is typical for long bursts. The redshifts are in the range of $z = 0.37$–0.98, so they are slightly more distant than the cases reported in other studies ($z = 0.03$–0.55).

6.1 The fraction of bursts with blackbody components

In the Models 1–2 comparison we found three new candidates (GRBs 061021, 061110A and 090814A) and we rediscovered GRBs 060218, 090618 and 101219B. So we found a blackbody component in six out of the 116 bursts (i.e. 5 per cent) with successful fits.

We will now shed light on the fraction of *Swift* bursts for which it is possible to recover a blackbody component like the one in GRB 101219B. In Section 3 it was found that such a blackbody component can be detected (with the *F*-test comparison of Models 1 and 2) if $z < 1.5$, $n_H < 0.4 \times 10^{22}$ cm^{-2} and the logarithm of the power-law normalization is below -0.5 (see Figs 1–3). Fig. 8 shows n_H versus z for all the bursts in our sample with successful fits. It is marked whether a bursts passes these detection criteria. We see that in 15 per cent, 15 out of 102 bursts, a detection will be possible. This calculation is, of course, only a rough estimate. The X-ray blackbody components need not all be like the one in GRB 101219B, and the limits we have used on z, n_H, Γ and power-law normalization are expected to be degenerate with each other. This calculation is, however, sufficient to establish that blackbody components only are detectable in a fraction of the bursts, even if such a blackbody component is present in all GRBs.

None of the new candidates found in this work has a optically confirmed SN. Note, however, that we excluded bursts which already are discussed in other works, including Paper I where several bursts with associated SNe are analysed.

7 CONCLUSION

We have first examined under which conditions a blackbody component, like the one proposed to be in GRB 101219B, can be recovered. At high redshift and in environments with intermediate or high column densities a detection of such a component will not be possible. We also find that it will be hard to recover a blackbody component, when a bright afterglow emission is present. We show that detection of a blackbody component only will be possible in a small fraction of all GRBs in our sample.

We have searched for blackbody components in all the *Swift* bursts with known redshift and created a list of bursts with possible blackbody components (GRBs 061021, 061110A, 081109, 090814A, 100621A and 110715A). They have temperatures, radii and luminosities similar to those found in previous studies of blackbody components in GRBs.

REFERENCES

Barthelmy S. D. et al., 2005, Nat, 438, 994
Burrows D. N. et al., 2005, Space Sci. Rev., 120, 165
Butler N. R., 2007, ApJ, 656, 1001
Campana S. et al., 2006, Nat, 442, 1008
Cano Z. et al., 2011, MNRAS, 413, 669
Cash W., 1979, ApJ, 228, 939
Chevalier R. A., Fransson C., 2008, ApJ, 683, L135
Cobb B. E., Bloom J. S., Perley D. A., Morgan A. N., Cenko S. B., Filippenko A. V., 2010, ApJ, 718, L150
Cucchiara A. et al., 2011, ApJ, 736, 7
de Ugarte Postigo A. et al., 2011, GCN Circ., 11579
Evans P. A. et al., 2009, MNRAS, 397, 1177
Fynbo J. P. U. et al., 2009, ApJS, 185, 526
Galama T. J. et al., 1998, Nat, 395, 670
Ghisellini G., Ghirlanda G., Tavecchio F., 2007a, MNRAS, 375, L36
Ghisellini G., Ghirlanda G., Tavecchio F., 2007b, MNRAS, 382, L77
Golenetskii S., Aptekar R., Mazets E., Pal'Shin V., Frederiks D., Cline T., 2006, GCN Circ., 5748, 1
Golenetskii S. et al., 2010, GCN Circ., 10882
Golenetskii S. et al., 2011, GCN Circ., 12166
Hjorth J., Bloom J. S., 2011, preprint (arXiv:1104.2274)
Hjorth J. et al., 2003, Nat, 423, 847
Jakobsson P., de Ugarte Postigo A., Gorosabel J., Tanvir N., Christensen L., Fynbo J. P. U., 2009, GCN Circ., 9797
Kalberla P. M. W., Burton W. B., Hartmann D., Arnal E. M., Bajaja E., Morras R., Pöppel W. G. L., 2005, A&A, 440, 775
Kouveliotou C., Meegan C. A., Fishman G. J., Bhat N. P., Briggs M. S., Koshut T. M., Paciesas W. S., Pendleton G. N., 1993, ApJ, 413, L101
Krühler T. et al., 2011a, A&A, 526, A153
Krühler T. et al., 2011b, A&A, 534, A108
Lampton M., Margon B., Bowyer S., 1976, ApJ, 208, 177
Li L.-X., 2007, MNRAS, 375, 240
Lipkin Y. M. et al., 2004, ApJ, 606, 381
Mazzali P. A. et al., 2006, Nat, 442, 1018
Milvang-Jensen B. et al., 2010, GCN Circ., 10876
Olivares E. F. et al., 2012, A&A, 539, A76
Page K. L. et al., 2011, MNRAS, 416, 2078
Patat F. et al., 2001, ApJ, 555, 900
Pian E. et al., 2006, Nat, 442, 1011
Piranomonte S., Vergani S. D., Malesani D., Fynbo J. P. U., Wiersema K., Kaper L., 2011, GRB Coordinates Network, 12164, 1
Protassov R., van Dyk D. A., Connors A., Kashyap V. L., Siemiginowska A., 2002, ApJ, 571, 545
Salvaterra R. et al., 2009, Nat, 461, 1258
Soderberg A. M. et al., 2006, Nat, 442, 1014
Sparre M. et al., 2011, ApJ, 735, L24
Starling R. L. C. et al., 2011, MNRAS, 411, 2792
Starling R. L. C., Page K. L., Pe'er A., Beardmore A. P., Osborne J. P., 2012, MNRAS, 427, 2950 (Paper I, this issue)
Starling R. L. C., Page K. L., Sparre M., 2012, in Roming P. W. A., Kawai N., Pian E., eds, Proc. IAU Symp. 279 Death of Massive Stars: Supernovae and Gamma-ray Bursts. Cambridge Univ. Press, Cambridge, p. 175
Tanvir N. R. et al., 2009, Nat, 461, 1254
Ukwatta T. N. et al., 2011, GCN Circ., 12160
Verner D. A., Ferland G. J., Korista K. T., Yakovlev D. G., 1996, ApJ, 465, 487
von Kienlin A., 2008, GCN Circ., 8505
Waxman E., Mészáros P., Campana S., 2007, ApJ, 667, 351
Wilms J., Allen A., McCray R., 2000, ApJ, 542, 914

This paper has been typeset from a TEX/LATEX file prepared by the author.